NATIONAL AERONAUTICS AND SPACE ADMINISTRATION

Technical Memorandum 33-711

Optical Properties of Mercury Ion Thruster Exhausts and Implications for Science Instruments

Kevin M. Monahan

Raymond Goldstein

JET PROPULSION LABORATORY

CALIFORNIA INSTITUTE OF TECHNOLOGY

PASADENA, CALIFORNIA

December 1, 1974

Prepared Under Contract No. NAS 7-100
National Aeronautics and Space Administration

Page intentionally left blank

PREFACE

The work described in this report was performed by the Space Sciences Division of the Jet Propulsion Laboratory.

ACKNOWLEDGMENTS

The authors are grateful to the operators of the JPL SEP Test Facility for their technical assistance during the period of data collection. In addition, we owe our thanks to Richard H. Parker and Douglas Clay for providing information and ideas essential to the preparation of this document.

CONTENTS

TABLES

FIGURES

FIGURES (Continued)

ABSTRACT

Emission from the exhaust plume of a 30 cm mercury ion thruster was measured from 160 to 600 nm as a function of axial and radial distance from the thruster discharge chamber. The spectrally dispersed absolute intensities were used to construct an empirical volume emission rate function. The function was integrated along a typical instrument field of view, and the resulting apparent brightness was compared with instrument sensitivities to evaluate the extent of optical interference.

Most of the emitted radiation came from UV lines of excited mercury atoms and ions, with no observable continuum emission. The intensity levels degraded rapidly with distance from the thruster so that optical interference was negligible for fields of view not intercepting the beam axis. The operation of only one instrument, a zodiacal photopolarimeter, was considered incompatible with simultaneous thruster operation.

I. INTRODUCTION AND SUMMARY

This work constitutes an empirical assessment of optical interference due to SEP exhaust plumes. The 30 cm mercury ion thruster used in the experiments is considered a likely candidate for use on future space missions. Emission and solar scattering from its exhaust are therefore a primary concern.[1] Scattering was measured by illuminating the exhaust beam with a solar equivalent flux. The results indicate that interference due to irradiation of the beam by sunlight will be insignificant relative to beam emission. Beam emission was measured from 160 to 600 nm and profiles were determined as a function of thruster gimbal angle. The emission was found to consist of discrete HgI and HgII lines with no observable continuum. The line intensities and beam profiles varied as a function of the principal thruster operating parameters: beam current, arc current, screen voltage, and accelerator voltage. The intensity data were used to construct an empirical volume emission rate function that could be readily integrated along any specified field of view to yield an apparent emission rate.

To evaluate the effect of beam emission rates on data collected by optical instruments on board a spacecraft, the calculated rates were compared to the minimum detectable signal (MDS), noise equivalent radiance (NER), or sensitivity of selected instruments. Viewing through the beam is a marginal or negligible problem for the MJS and AAFE UV-Spectrometers; Imaging; the MJS Optical Particle Detector; the MJS Infrared Spectrometer; and the Viking Infrared Radiometer. Of all the instruments, only a zodiacal light/photopolarimeter is severely limited by beam emission when viewing in or near the plume. The OSO Spectroheliograph being considered for a proposed SEP Out-of-the-Ecliptic Mission

is insensitive to photon energies below the ionization limits of HgI and HgII. Nonetheless, the possibility of EUV emission due to thruster arcing or excitation of highly ionized mercury has not been ruled out; and an investigation of this spectral region is warranted.

II. EXPERIMENTAL

A. The 30 cm Ion Thruster and Test Facility

A simplified block diagram of the mercury ion thruster operation is shown in Figure 1. Liquid mercury is vaporized and allowed to flow into the discharge chamber. Energetic electrons generated by the discharge cathode are trapped by a divergent magnetic field in the main chamber and produce mercury ions by electron impact. The positive ions are then accelerated out of the chamber by an applied electric field as shown in Figure 2. To avoid buildup of space charge on the thruster, the ion beam is then neutralized by electrons emitted from the plasma bridge neutralizer (Figure 3). At distances far from the thruster the mercury ions in the plasma beam will have kinetic energies (in electron volts) nearly equal to the screen potential V_s (typically $\sim$ 1 keV). Relevant operating parameters[2] of a typical 30 cm thruster are listed in Table 1.

The ion thruster test chamber is 2.3 m in diameter and 4.6 m in length excluding front and rear end bells. The 30 cm ion thruster was mounted inside the front end bell so that the center of the discharge chamber was approximately 0.5 and 2.0 m from the view axis of the ports used for observation. During periods of thruster operation the test chamber is maintained at 10^{-4} to 10^{-5} N/m^2. Since care must be taken to guard the vacuum all observations are made through 0.5 cm thick by 10 cm diameter fused silica windows with transmittance

down to 160 nm. The expelled mercury is collected by a liquid nitrogen cooled surface in the chamber.

B. Solar Simulation

An effort was made to determine the relative importance of solar ultraviolet scattering from the mercury ion thruster beam.

The experimental arrangement is shown in Figure 4. The xenon illuminator and the photomultiplier collimator axes intersect at an angle of 105^{o} and lie in a plane perpendicular to the beam axis at 2.0 m from the thruster. The xenon lamp is designed to provide near solar equivalent intensities (Table 2) within the 0.008 sr acceptance cone of the PMT collimator. An E.M.I. 6256B photomultiplier with a salicylate coated pyrex filter and fused quartz vacuum window was used to measure the light intensity. This detector combination is sensitive from the fused quartz cutoff at 160 nm to the long wavelength cutoff of the phototube near 600 nm. A stepping motor-actuated gimbal rotates the thruster on an axis parallel to the collimator so that beam alignment can be accomplished by finding a maximum on the beam emission profile.

Our results are summarized in Table 3. With such an intense source most of the signal measured was due to scattering from the walls of the test chamber. Switching the beam on produced a 6% reduction in the observed change of intensity due to the xenon lamp. Assuming the difference is an absorption or scattering effect, it represents less than 3% of the normal beam emission intensity and should not produce interference.

C. Parametric Dependence of Beam Profiles

Using the same setup as described above (with the omission of the xenon lamp) beam profiles were measured at 2.0 m from the thruster. The thruster was

gimballed over a range of ± 0.2 rad to obtain the curves shown in Figures 5 and 6. Our data show the profiles to be parabolic in Θ near the core and exponential in the wings. This observation is in qualitative agreement with measurements of ion density profiles for mercury ion thrusters.[3]

Figure 5 shows relative intensity as a function of angle Θ and beam current I_B. At 0.2 rad the LAB-FOV is essentially outside the region of emission from the exhaust beam. The background intensity is the result of scattered light from the discharge arc. Scattered light from the arc is directly proportional to beam current since the discharge current I_D is nominally maintained at 5 I_B. For any given I_B, the scattered light level can be obtained from the limit of zero screen potential, and subtracted from the data.

Figure 6 shows relative intensity as a function of Θ and screen potential V_s. The data are taken at constant I_B so that a single background scattering correction suffices for all three curves. Higher screen voltages produce better beam collimation and the intensity at $\Theta = 0$ rad is roughly proportional to screen voltage. The total integrated intensity also increases with screen voltage. This behavior can be taken as evidence for collisional excitation taking place near the core of the exhaust plume.

D. Spectral Analysis of the Beam Emission

To obtain the wavelength dependence of exhaust plume optical interference it was necessary to disperse the radiation emitted. The phototube in the above setup was replaced with an optical system consisting of a 0.5 m focal length scanning monochromator fitted with a collimator. The grating was completely filled and no condensing lens was used with the extended source. An E.M.I. 6256B photomultiplier with an S-13 response was used in conjunction with a

partially transmitting, sodium salicylate coated, pyrex window. This particular combination is sensitive from 600 nm to the extreme ultraviolet and can be attached to a vacuum monochromator without further modification. The monochromator and detector were calibrated against a 1000-watt quartz-iodine, tungsten-filament lamp supplied by the National Bureau of Standards.

A single 30 cm mercury ion thruster was mounted at one end of the 2.3 m diameter test chamber. The beam was observed through a 10 cm fused silica window at distances of 0.5 m and 2.0 m from the thruster measured along the beam axis. At both locations the viewing axis was perpendicular, intercepting the beam in the region of maximum emission intensity.

Figure 7 is a typical 1.0 A emission spectrum taken at reduced sensitivity. The five strongest HgI lines are indicated. The bright feature at 507.4 nm is the 253.7 nm resonance seen in second order. Also observable at higher sensitivity is the HgII 281.5 nm transition.

E. Determination of Axial Decay Rates

The decrease in the intensity of the five strongest HgI lines and the HgII line at 281.5 nm was measured as a function of distance from the thruster. Intensities at 0.5 m and 2.0 m were compared; the sharp decrease of intensity at 2.0 m was assumed to be nearly exponential although it was not possible to verify this assumption rigorously by obtaining data at a third point along the beam axis. Measurements of primary axial ion current density also show exponential decay for distances greater than about four thruster radii. Table 4 shows the decay of selected emission lines of HgI and HgII (281.5 nm) with distance. The 365.0 nm and 281.5 nm lines are anomalous in the sense that, relative to the average, the former decays twice as rapidly and the latter eight times more

slowly. The slow decay of 281.5 nm intensity identifies it as a forbidden transition from the $^2D_{5/2}$ metastable level of singly ionized mercury rather than the MoII 281.6 nm impurity line. This state is probably populated by collisions in the discharge chamber of the thruster.

F. Absolute Intensity Calibration

The monochromator-phototube combination was calibrated down to 250 nm by means of a quartz envelope light source supplied by the National Bureau of Standards (Table 5). The spectral radiance of the NBS lamp is considerably less than that of the xenon lamp in the short wavelength region (Table 2). For this reason, calibration in the short wavelength region is more subject to error due to scattering of intense long wavelength radiation in the monochromator. A scattering correction was applied to the calibration by measuring the observed intensity at 180.0 nm where the lamp output is negligible. In Table 6 are listed absolute radiances for the five strongest HgI lines and the 281.5 nm HgII line. These data are unique since they are the only optical measurements taken at close proximity (0.5 m) to a 30 cm thruster. Table 7 compares data obtained by Milder and Sovey[4] at 1.8 m with present results at 2.0 m. Agreement is quite close above 400 nm, but absolute radiance values differ by a factor of two for the 365.0 and 281.5 nm lines. In addition, Milder and Sovey predict a very high value for the 253.7 nm line based upon their second order measurements. Our ratio of 281.5 nm to 253.7 nm radiation varies from theirs by more than an order of magnitude in a region where our spectral sensitivity is only a slowly varying function of wavelength. It is most likely due to differences in thruster construction and operating parameters.

G. Parametric Dependence of Spectral Features

It was necessary to measure the dependence of spectral features on thruster operating parameters to ensure the general applicability of the bolometric profile data. Table 8 represents a study of line intensity as a function of exhaust beam current. Emission varies almost linearly with beam current above 1.0 A, but drops off rapidly at low current levels. With the screen voltage at zero, there is no beam; ions and neutrals migrate into the chamber by thermal effusion. If the arc remains on for long periods under such conditions, the plasma density near the thruster can increase until the radiation output is over an order of magnitude greater than normal. The plasma temperature increases also, and the shorter wavelength emissions are favored (Table 9). The relative intensity of the 253.7 nm HgI line was measured as a function of discharge current (beam off); and the signal was found to be directly proportional to current in the normal operating range (Table 10).

H. Emission Below 200 nm

Measurements were made to obtain "order of magnitude" estimates of beam emission intensity at shorter wavelengths. A 0.5 m focal length vacuum monochromator with a sodium salicylate coated photomultiplier was set up to observe the beam through a sapphire window at approximately 0.5 m from the thruster. Since the quantum efficiency of sodium salicylate is nearly constant[5] in the region from 160 to 200 nm, the instrument sensitivity is a slowly varying function of grating efficiency.

The results below 200 nm given in Table 11 for several values of the I_D/I_B ratio should be considered accurate to within a factor of ten. Lowering the discharge current I_D with respect to a constant beam current I_B produces

more radiation from excited neutrals due to a higher neutral/ion density ratio. Thus, it may be possible to use a UVS to monitor thruster performance (i.e., utilization efficiency).

I. General Observations

Beam emission intensities were subject to a variety of periodic, aperiodic, and sporadic instabilities. These could usually be traced to variations in thruster operating parameters. A periodic change in the bolometric light intensity (integrated from 160 to 600 nm) is often due to large amplitude oscillations in mercury vapor flow. During startup of the thruster, damped aperiodic instabilities in emission intensity may arise as the cathode vaporizer control loop begins to operate. Under certain conditions high voltage arcing can occur between the acceleration and screen grids. Momentary sporadic increases in light intensity are observed during arcing (Figure 8). All of these intensity variations tend to take place during relatively short time intervals and would contribute little to optical interference unless the device were being cycled rapidly on and off.

Some evaluations of thruster performance could be made visually. Arcing was easily seen as bright sparks flying off the grids. In addition, when only the arc discharge was operating a luminous blue haze could be seen in the vicinity of the thruster, as shown in the photograph (Figure 9a). It can be seen that the visible emission intensity decreases rapidly with radial and axial distance from the thruster. When high voltage is applied to the grids and an ion beam is extracted, this haze disappears as shown in part (b) of the Figure.

III. IMPACT ON OPTICAL INSTRUMENTATION

A. Sources of Emission

The emitting regions of primary concern here are the main discharge chamber of the thruster and the exhaust plume. In the former, Hg atoms are ionized and excited by electron impact. In addition, an unknown quantity of neutrals may be excited by electron impact and by ion-atom collisions. These neutrals move out of the thruster via a combination of effusion and entrainment processes so that a considerable amount of the observed radiation can be expected to come from excited states of HgI. Although the radiation emitted from the discharge chamber is much more intense than that observed in the plume, it presents a relatively small obstacle to optical observations, primarily because normal spacecraft geometries are such that the interior of the discharge chamber would not lie within an instrument FOV. A simple precaution should be taken that no highly reflective surfaces are placed simultaneously in view of both an optical instrument and the mercury discharge. This injunction applies especially to an ultraviolet spectrometer since HgI and HgII radiate mainly in the blue and ultraviolet.

In the thruster plume, the principal sources of emission can be listed as follows:

1) Decay of excited states populated by electron impact and collisional excitation in the discharge chamber.

Sensitive lines such as the HgI 184.9 nm may have very short optical depths. Radiation may be "trapped" in the plume so that the apparent lifetimes of excited states appear much longer than in the case of a tenuous medium (one having a large optical depth relative to the dimensions of the spacecraft).

Also, if the ion and neutral temperatures decrease with axial and radial distance from the thruster, considerable line reversal (reabsorption by a cooler region of the vapor) could occur contributing to the error of intensity measurements. Fortunately, most of the strong HgI and HgII lines are sharp having small natural line widths relative to their Doppler widths. Degradation of intensity through line reversal should therefore be small.

2) Excitation by inelastic collision within the exhaust plume.

The exhaust plume under normal conditions is a neutral plasma composed of varying amounts of neutral, singly, and doubly ionized mercury atoms. Assuming accumulation of space charge on the thruster is effectively neutralized via the plasma bridge, the HgII and HgIII ions will have kinetic energies V_s and $2V_s$ respectively where $V_s \approx 1000$ eV. Their velocities (Figure 10) can be found by the usual relation

$$v = \sqrt{\frac{2V_s}{m}} \tag{1}$$

where m is the atomic mass of Hg. Thus, the approximate number density of single ions is given by

$$n = \frac{I_B}{\pi R^2 e}\sqrt{\frac{m}{2V_s}} \tag{2}$$

where R is the thruster radius. Ion number densities calculated from the relation are plotted in Figure 11. The process of obtaining these two important beam characteristics v and n from known thruster parameters V_s and I_B is not quite so straightforward as it seems. I_B is actually the sum of single and double ion currents. Measurements done in this laboratory indicate that typical $I_B(Hg^{++})/I_B(Hg^{+})$ ratios lie between 0.10 and 0.15. The ratio $n(Hg^{++})/n(Hg^{+})$ will

therefore be 0.7 times as great, indicating that of the charged particles in the beam well over 90% are singly ionized.

The percentage of neutrals in the beam is not well known, but optical measurements have made order of magnitude calculations possible. The Einstein-Boltzman equation for the photon emission rate of a spectral line is

$$F = Z^{-1} \; ngAe^{-E/kt} \tag{3}$$

where Z is the partition function for any particular atom or ion, n is the number density, g is the statistical weight of the upper level, A is the Einstein transition probability, E is the energy of the photon, k is Boltzman's constant, and T is the absolute temperature of the source. This equation only applies rigorously to sources in "thermal equilibrium;" otherwise, calculations of the $n(Hg^+)/n(Hg^o)$ ratio will be adversely affected to an extent based on the prevalence of non-thermal excitations. A reasonable estimate of the beam temperature can be made by plotting $\ln \frac{F}{gA}$ versus E; the slope of the best straight line drawn through the points (Figure 12) will be -1/kT, and the intercept at $\ln \frac{n}{Z}$ will yield a value for the number density of neutrals in the beam. Temperatures obtained in this manner are near 10^4 K, in order of magnitude agreement with measurements of beam electron temperatures ($\sim$ 4000 K).[6] Densities obtained from the intercepts and published values of the partition function[7] lie near 10^{10} cm^{-3} yielding an $[Hg^o]/[Hg^+]$ concentration ratio of $\sim$ 1, which explains the large amount of neutral emission observed.

An estimate of the collision rate R for ions with atoms can be made from

$$R = [Hg^+] \; v \; [Hg^o] \; \sigma \tag{4}$$

If $[Hg^+]$ and $[Hg^o]$ are 3×10^9 cm^{-3}, the ion velocity v is 3×10^6 cm s^{-1}, and the collision cross section σ is 10^{-16} cm^2, then R will be of order 3×10^9 s^{-1} cm^{-3}. The high rate suggests that a large fraction of the emission may be produced by inelastic collisions in the exhaust beam.

3) Recombination and charge transfer

Since some loss of energy is necessary for recombination to take place, the recombining ion-electron pair must either collide with a third body or radiate (radiative recombination). Thus the maximum energy available for conversion into photons is 18.75 eV for HgII and 10.39 eV for HgI, their respective ionization potentials. These energies are more than sufficient to account for the observed emission; for example, the HgI 184.9 nm and the HgII 165.0 nm lines correspond to 6.7 and 7.5 eV photons respectively. In comparison, the neutral-double ion charge transfer process yields an excess energy of 8.4 eV, again, adequate to explain the observed lines. Very little is known about optical emission associated with charge transfer reactions of mercury.[8]

4) Cascade processes

Although not a primary excitation mechanism, cascade processes can populate metastable states such as the HgI $^3P_2$ and the HgII $^2D_{5/2}$ or enhance the emission of various allowed transitions. The $^3S_1 \rightarrow {}^3P_1$ transition of HgI at 435.8 nm, for example, contributes significantly to the intensity of the 253.7 nm intersystem resonance line. Energy level diagrams[9] for HgI and HgII detailing the cascade and resonance transitions observed in mercury ion thrusters are shown in Figures 13 and 14.

Table 12 summarizes the principal mechanisms of optical excitation in the exhaust beam of mercury ion thruster. The resonant charge transfer[10]

should have a very high cross section ($\sim 10^{-14} - 10^{-15}$ cm^2). Other inelastic scattering may have cross sections nearly as large, but recombination (radiative or third body) is significantly less likely. In any case, the energy released by electrons cascading down to their ground states is the result of a complex process. Therefore, an empirical approach to the modeling of exhaust beam emission has been adopted.

B. A Photometric Function for the Exhaust Beam Emission

The following describes the empirical derivation of a volume emission rate function for emission from a 30 cm mercury ion thruster. The function is used to calculate the impact of beam emission on observations made with a typical Mariner type ultraviolet spectrometer. The interference is negligible for any reasonable view axis.

1) Volume Emission Rate

An empirical volume emission rate $F(r,z)$ can be derived directly from the exhaust beam emission data. The coordinates shown in Figure 15 are thruster-centered with the optical beam limits at $\Theta = 0.2$ rad. Data were obtained only for $\Theta \leqslant 0.2$ rad; the emission outside that range is small. No attempt is made to determine whether the emission is isotropic, or whether the photons are reabsorbed or scattered. The measured radiances I appear to decay exponentially with axial distance z from the thruster ($z \geqslant 0.5$ m). As a function of Θ, the measured radiances exhibit a characteristic parabolic core at small Θ and decay exponentially for large Θ. This behavior is similar to that observed for the ion density distribution along the beam.

An excellent fit to the data can be made using the empirical relation

$$F(r, z) = F(0, z_0)\ e^{-a(z - z_0)}\ e^{-br^2/z^2} \tag{5}$$

where r^2/z^2 has been substituted for θ^2, an accurate approximation for small angles. A Taylor series expansion of the last term yields the required parabolic dependence for small θ:

$$e^{-br^2/z^2} \approx 1 - br^2z^{-2} \tag{6}$$

The constants a and b can be determined from axial decay and profile measurements respectively, while $F(0, z_0)$ can be obtained from absolute intensity measurements at z_0.

At the profile plane determined by $z = z_0$ the function F(r,z) becomes

$$F(r, z_0) = F(0, z_0)\ e^{-br^2/z^2_0} \tag{7}$$

The observed radiance I_{LAB} can be calculated from the distribution by integrating over r.

$$4\pi I_{LAB} = F(0, z_0) \int_{-0.2z_0}^{0.2z_0} e^{-br^2/z^2_0}\, dr \tag{8}$$

The values of b determined from the profile shapes are sufficiently large that the limits on the integral can be replaced by $\pm \infty$. Thus we have the relation

$$F(o, z_0) = \frac{4\sqrt{\pi b}}{z_0} \quad I_{LAB} \tag{9}$$

Since the profiles are not spectrally dispersed, the constant b represents an average value and will be considered independent of wavelength. The b values are somewhat dependent upon beam current and screen voltage but for a nominal 1.5 A beam at 1100 volts, b is equal to 160.

The constants $a = a_\lambda$ are wavelength dependent and evaluated by means of the expression

$$a_\lambda = \frac{1}{1.5m} \ln \left[\frac{I_{LAB}\ (0.5m)}{I_{LAB}\ (2.0m)} \right] \tag{10}$$

The values of a_λ and $F(0, z_0)$ as well as the respective Einstein transition probabilities, are displayed in Table 13.

2) Optical Interference Calculation

An upper limit can now be calculated for UVS optical interference at 365.0 nm if the following assumptions are made.

1) The UVS-FOV is parallel to the thruster beam axis and separated by a distance of $r_0 = 1$ m.
2) The thruster is operating at 1.5A beam current with 1100V screen potential.
3) A typical UVS detection limit is a radiance of $\frac{10^{12}}{4\pi}$ photon $m^{-2}\ s^{-1}\ sr^{-1}$.

The apparent emission rate can be calculated by evaluating the integral

$$4\pi\, I_{UVS} = \int_{z = 5r_0}^{\infty} F(r_0, z)\,dz \qquad (11)$$

At $r_0 = 1$ and $\lambda = 365.0$ nm

$$F(1, z) = (6.6 \times 10^{14} \text{ photon m}^{-3} \text{ s}^{-1}) e^{-3(z - z_0)}\, e^{-160/z^2}$$

An upper limit on the integral can be obtained by setting the last factor in the integrand equal to one. The apparent emission rates in 365.0 nm are 2×10^{10} photon m^{-2} s^{-1} and 5×10^{11} photon m^{-2} s^{-1} for the UVS-FOV and the LAB-FOV ($z_0 = 2.0$ m) respectively.

The beam emission from a 30 cm mercury ion thruster does not produce sufficient intensity to interfere with UVS measurements at normal experimental fields of view. Even for instruments with detection limits lower than 10^{12} photon m^{-2} s^{-1}, the discrete HgI line spectrum can easily be subtracted out. On the other hand, if UVS monitoring of thruster performance is required, the instrument mount must be so configured that the UVS-FOV can intersect the beam axis at distances less than 2 m from the thruster. Measurements of apparent emission rate at 0.5 m from the thruster yield 5×10^{13} photon m^{-2} s^{-1} at 365.0 nm (LAB-FOV).

C. Effect of Potential SEP Optical Interference on Specific Scientific Instruments

The level of optical interference produced by a mercury ion thruster is a function of its operating condition. Needless to say, no interference will be generated when the thruster arc and beam are off; and this would be the ideal occasion for experimentation. Either cometary rendezvous or out-of-the-ecliptic (O/E) missions, however, may require thrusting during prime data collection periods. Thus, the thruster arc and beam will be on much of the time; and the following qualified assessment of optical interferences will be based upon this operating condition. The qualification is this:

ultraviolet and visible data should not be taken in the direction of thruster effluent if the beam is off and the arc has remained on for more than a few minutes (Figure 9a), nor should any instrument FOV intersect the beam axis. For other cases, as our measurements indicate, the SEP exhaust will produce only negligible or marginal interference with scientific instruments.

Several components (Table 14) of the science instrument packages proposed for cometary, O/E, and MJS missions have been selected (on the Basis of sensitivity and wavelength range) for the assessment of optical interference:

1) The UV Spectrometer is a moderately sensitive narrow bandpass instrument (~1.5 mm). Although the strong HgI and HgII emission lines at 165.0, 184.9, 194.2 and 253.7 nm lie within the MJS-UVS range, all exhibit an apparent emission rate less than 10^{10} photon m^{-2} s^{-1} for an FOV parallel to and 1 m from the beam axis. The minimum detectable signal (MDS) is of order 10^{11} photon m^{-2} s^{-1} so that no serious optical interference is expected from solar electric propulsion.

2) Both the Optical Particle Detector (OPD) and the Zodiacal Photometer are very sensitive braodband instruments. The instruments will observe, when viewing along the UVS-FOV, an apparent emission rate of order 10^{11} photon m^{-2} s^{-1} over all HgI and HgII emission wavelengths. Although each OPD sensor can detect such interfering levels very easily, it is a coincidence experiment sensitive to light pulses only in the overlap region of its four conical FOV directions. Care should be taken that the FOV overlap does not lie within the exhaust plume when the thruster is operating.

3) The Zodiacal Photometer is the instrument most susceptible to optical interference. Having nearly the same wavelength range and sensitivity as the OPD, it can easily detect emission when viewing close to the exhaust

plume. Since the photometer is not dispersive, the contribution from plume emission cannot be easily removed from the data. Therefore, we suggest that photometer FOV not be allowed to intersect the exhaust plume while the thruster is operating.

4) Imaging and Filter Photometry are low sensitivity broadband experimets. No interference problems are anticipated for normal camera exposure times.

5) The Infrared Spectrometer and IR Radiometer are moderately sensitive instruments. Since HgI and HgII emit primarily in the blue and UV, and no comparable continuum up to 600 nm has been observed in our experiments, data from these devices will be largely unaffected by the plume. A short wavelength range of the IR Radiometer used for determining albedo will not be significantly affected because beam emission will be negligible relative to cometary or planetary albedo intensities.

6) The Spectroheliograph is sensitive in the EUV and soft x-ray region. Nothing is currently known about emission from the thruster in this region, except that, with $V_s \approx 2000$ V and $V_a \approx 1000$ V, the thruster is theoretically capable of producing photons with wavelengths as short as 0.4 nm. Such radiation would propagate solely from the grids of the thruster; thus, normal care should be taken that the grids do not lie within the Spectroheliograph FOV. Laboratory measurements in the EUV may be justified.

All of the instruments mentioned above may be influenced by absorption in the thruster beam. The low beam densities and the relative insignificance of solar scattering compared to beam emission indicate that this will not be a problem. The Zodiacal Photometer seems to be the only instrument seriously affected by SEP operation, and observations within the thruster hemisphere may have to be relegated to the periods of coasting.

REFERENCES

1. Parker, R. H., et al., A Study of the Compatibility of Science Instruments With the Solar Electric Propulsion Space Vehicle, JPL TM 33-641, Pasadena, California, 15 October, 1974.

2. Sellen Jr., J. M., et al., Solar Electric Propulsion/Instrument/Subsystems Interaction Study, Final Report, Report 22878-6007-RU-00, TRW Systems, Redondo Beach, California, March 30, 1973.

3. Hall, David F., Electrostatic Propulsion Beam Divergence Effects on Spacecraft Surfaces, Final Report, Vol. II, Report 11985-6002-RU-00, TRW Systems, Redondo Beach, California, January 17, 1973.

4. Milder, Nelson L., and Sovey, James S., "Star Tracking through the Exhaust Beam of Mercury Bombardment Thrusters," J. Spacecraft 10, 47 (1973).

5. Samson, J. A. R., Techniques of Vacuum Ultraviolet Spectroscopy (John Wiley and Sons, New York, 1967).

6. Sellen, J. M., Jr., "Electric Propulsion Interactive Effects with Spacecraft Science Payloads," Paper 73-559, AIAA/AGU Space Science Conference: Exploration of the Outer Solar System, Denver, Colorado, July 1973.

7. Claas, W. J., Recherches Astron. Obs. Ultrecht 12, 1 (1951).

8. Vroom, D. A., Cross Sections for Charge Transfer between Mercury Ions and Other Metals, CR 8095-013, Atomic Physics Branch, Intelcom Rad Tech, San Diego, California, July 3, 1974.

9. Milder, N. L., and Sovey, J. S., "Preliminary Results of the Spectrographic Analysis of Kaufman Thruster," Paper 70-176, AIAA 8th Aerospace Sciences Meeting, New York, N. Y., Jan. 19-21, 1970.

10. Knewstubb, P. F., Mass Spectrometry and Ion-Molecule Reactions, University Press, Cambridge, 1969).

11. Corliss, C. H., and Bozman, W. R., Experimental Transition Probabilities for Spectral Lines of Seventy Elements, National Bureau of Standards.

12. Investigation Descriptions for the 1977 Mariner Jupiter/Saturn Missions, JPL Internal Document, 5 April 1973.

13. Newburn, R. L., ed., Science Rationale and Instrument Package for a Slow Flyby of Comet Encke, JPL Internal Document, 1 June 1973.

14. Sterk, A. A., et al, Extreme Ultraviolet and x-ray Spectroheliograph for OSO-7, NASA CR-122502, 20 January 1972.

TABLE 1

OPERATING PARAMETERS FOR THE 30 cm THRUSTER

Normal Operating Parameters	30 cm thruster
V_s, Screen Potential (ion accelerating potential)	+ 500 to 2000V
V_a, Accelerator Grid Potential ($\|V_a\|+\|V_s\|$ = ion extraction potential)	~ -1000V
I_B, Beam Current (mercury ion current)	0.5 to 1.5A
I_D, Arc Discharge Current (nominal $\approx 5\ I_B$)	5 to 15A

TABLE 2*

XENON LAMP OUTPUT COMPARED TO SOLAR FLUX

Wavelength (nm)	Lamp Output ($\mu W/cm^2$-nm)	Solar Flux ($\mu W/cm^2$-nm)
200	34	(1.2)
220	77	(5.7)
240	100	(6.1)
260	110	(13)
280	117	(18) 22
300	120	62
320	122	81
340	124	112
360	126	118
380	128	123
400	131	140
420	135	193
440	137	188
460	187	218
480	164	216
500	149	207
520	151	193
540	149	199
560	148	193
580	148	193
600	144	188

*Data in parentheses are from JPL Technical Report No. 32-951. Otherwise the data are converted from values supplied by Varian/Eimac, the manufacturers of the VIX-150-UV xenon lamp. Lamp output is that calculated at the center of the vacuum chamber. Solar flux is that observed at 1 A.U.

TABLE 3*

SOLAR SCATTERING RESULTS

Thruster (Arc on)	Intensity		
	Lamp off	Lamp on	Change
Beam off	0.07	0.43	0.36
Beam on	0.66	1.00	0.34

*Change in exhaust beam relative emission intensity due to external illumination in excess of 1 solar constant.

TABLE 4*

INTENSITY RATIOS FOR SELECTED MERCURY LINES

Wavelength	Relative Intensities at Distance from Thruster		Ratio
(nm)	0.5m	2.0m	2.0m/0.5m
253.7	0.18	0.0047	0.026
281.5	0.03	0.0046	0.153
365.0	4.27	0.0460	0.011
404.7	0.95	0.0200	0.021
435.8	3.32	0.0620	0.019
546.1	2.06	0.0370	0.018

*Measured Hg line relative intensities as a function of distance from the thruster along the beam axis. Detector geometry is identical at both ports.

TABLE 5*

OUTPUT OF THE QUARTZ-IODINE TUNGSTEN FILAMENT LAMP

Wavelength (nm)	Quartz Lamp Output ($\mu W/cm^2$-nm)
250	0.017
260	0.030
270	0.052
280	0.084
290	0.13
300	0.18
320	0.35
350	0.81
370	1.26
400	2.19
450	4.41
500	7.48
550	10.9
600	14.3

*Data supplied by the National Bureau of Standards.

TABLE 6*

ABSOLUTE RADIANCE AT 0.5 m FROM THE THRUSTER

Wavelength (nm)	Spectral Sensitivity	Measured Intensity	Absolute Radiance W/cm^2 - sr
253.7	0.32	0.042	9×10^{-9}
281.5	0.37	0.008	2×10^{-9}
365.0	1.00	1.000	7×10^{-8}
404.7	1.78	0.220	9×10^{-9}
435.8	2.54	0.780	2×10^{-8}
546.1	1.73	0.480	2×10^{-8}

*Data were taken at 0.5m distance and 1.5A beam current. Acceptance angle of the instrument collimator was 0.008 sr. Spectral sensitivity and measured intensity are normalized to unity at 365.0 nm.

TABLE 7*

ABSOLUTE RADIANCE AT 2.0 m FROM THE THRUSTER

Wavelength (nm)	Absolute Radiance (W/cm^2 - sr)	
	1.8m*	2.0m
253.7	—	3×10^{-10}
281.5	7×10^{-10}	3×10^{-10}
365.0	2×10^{-9}	8×10^{-10}
404.7	2×10^{-10}	2×10^{-10}
453.8	4×10^{-10}	4×10^{-10}
546.1	4×10^{-10}	4×10^{-10}

*Reference 4. All data taken at 1.5A beam current.

TABLE 8*

PARAMETRIC DEPENDENCE OF LINE INTENSITIES ON BEAM CURRENT

Wavelength (nm)	Beam Current		
	0.5A	1.0A	1.5A
253.7	0.33	1.00	1.43
365.0	0.34	1.00	1.50
404.7	0.33	1.00	1.50
435.8	0.31	1.00	1.39
546.1	0.33	1.00	1.50

*Hg I line intensities as a function of beam current. Intensity of each line is normalized to 1.0A beam. Distance is 0.5 m.

TABLE 9*

LINE INTENSITY RATIOS OF BEAM ON AND BEAM OFF

Wavelength nm	Intensity Ratio Beam On/Beam Off
253.7	0.17
365.0	0.66
404.7	0.92
435.8	2.00
546.1	1.38

*Measured at 0.5 m with I_B = 1.0A, I_D = 5.0A.

TABLE 10*

PARAMETRIC DEPENDENCE OF 253.7 nm LINE INTENSITY ON ARC CURRENT

Arc Current Amps	Intensity 253.7 nm
0.0	0.0
2.5	1.6
5.0	3.2

*Measured at 0.5 m with $V_s = 0$, $V_a = 0$, $I_B = 0$.

TABLE 11*

RADIANCES OF THE HgI and HgII RESONANCE LINES

Wavelength (nm)	Radiance at I_D/I_B Ratio (10^{-9} W/cm^2-sr)		
	7.0	5.4	4.1
Hg I 253.7	8.0	9.0	14.
Hg II 194.2	1.6	1.6	2.3
Hg I 184.9	2.6	3.2	4.8
Hg II 165.0	0.8		

*I_B is constant at 1.5A

TABLE 12

REACTIONS LEADING TO EXCITED STATES OF HgI and HgII

Inelastic Collisions

Hg^{++} (K.E.) + Hg^{+} → Hg^{++} + Hg^{+*}

Hg^{++} (K.E.) + Hg → Hg^{++} + Hg^{*}

Hg^{+} (K.E.) + Hg → Hg^{+} + Hg^{*}

Charge Transfer

Hg^{++} + Hg → Hg^{+} + Hg^{+*}

Hg^{+*} + Hg → Hg^{+} + Hg^{*} (resonant)

Recombination

Hg^{++} + e → Hg^{+*}

Hg^{+} + e → Hg^{*}

Cascade

Hg^{+**} → Hg^{+*} + $h\nu$

Hg^{**} → Hg^{*} + $h\nu$

*Asterisk indicates an electronically excited species

TABLE 13

VOLUME EMISSION RATE PARAMETERS

λ (nm)	gA* ($10^8 s^{-1}$)	a_λ (m^{-1})	$F(o, z_o)$ (10^{12} photon $m^{-3}s^{-1}$)
253.7	3.5	2.4	170
281.5	-	1.2	190
365.0	64.	3.0	660
404.7	36.	2.5	180
435.8	86.	2.6	390
546.1	86.	2.6	490

*Reference 11.

TABLE 14*

OPTICAL INSTRUMENTS SUBJECT TO POTENTIAL SEP INTERFERENCE

INSTRUMENT	WAVELENGTH RANGE	SENSITIVITY
UV Spectrometer		
MJS 77	40 - 180 nm	4×10^{11} photon m^{-2} s^{-1}, MDS
AAFE	100 - 340 nm	$\sim 10^{11}$ photon m^{-2} s^{-1}, MDS
MJS Photopolarimeter (O/E Zodiacal Photometer)	220 - 730 nm	$\sim 10^{8}$ photon m^{-2} s^{-1}, MDS at 560 nm
Optical Particle Detector (Sisyphus)	300 - 700 nm	$\sim 10^{8}$ photon m^{-2} s^{-1}, MDS at 560 nm Strong rejection outside conical FOV overlap.
Imaging (Filter Photometry)	300 - 600 nm	Variable with exposure time. Low Sensitivity. High spatial resolution.
Infrared Spectrometer	3μm - 50 μm	
Interferometry		5×10^{-10} $Wcm^{-2}sr^{-1}$, NER
Radiometry		8×10^{-9} $Wcm^{-1}sr^{-1}$, NER
IR Radiometer (Modified Viking IRTM)	0.3 μm - 40 μm	
Spectroheliograph (OSO -7)		
H - alpha	126 nm	5×10^{-3} counts/photon • s^{-1}
EUV	17 - 40 nm	
X-ray	0.2 - 1.6 nm	

*References 12, 13, and 14.

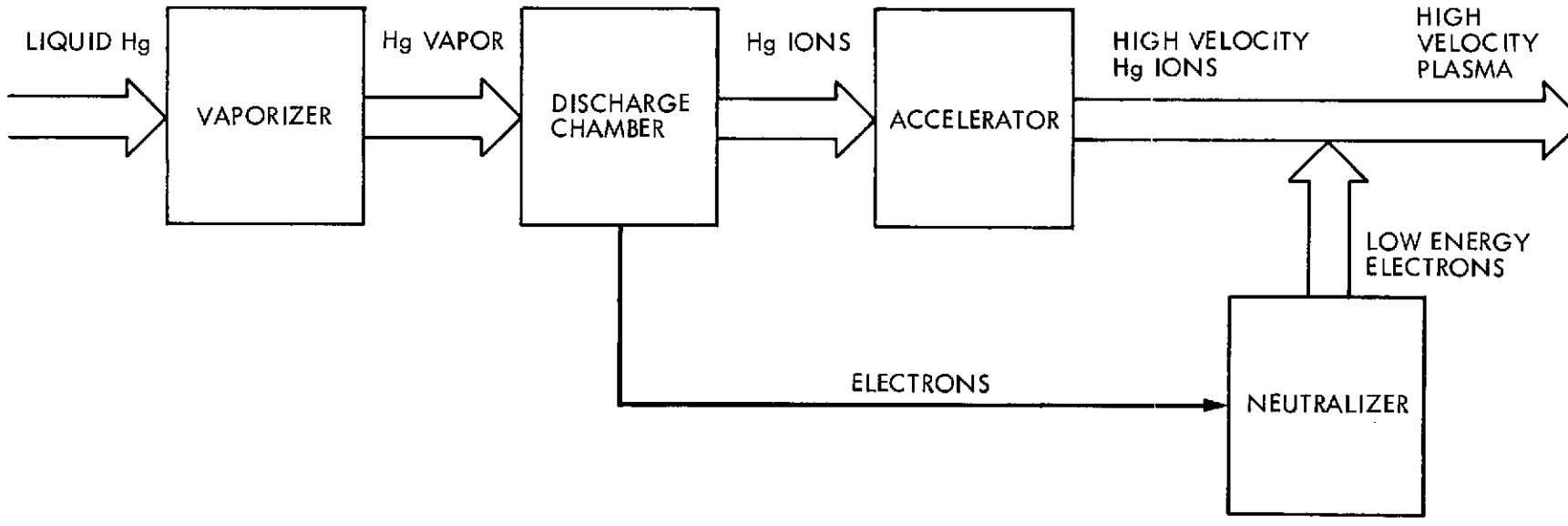

FIG. 1 ION THRUSTER BLOCK DIAGRAM

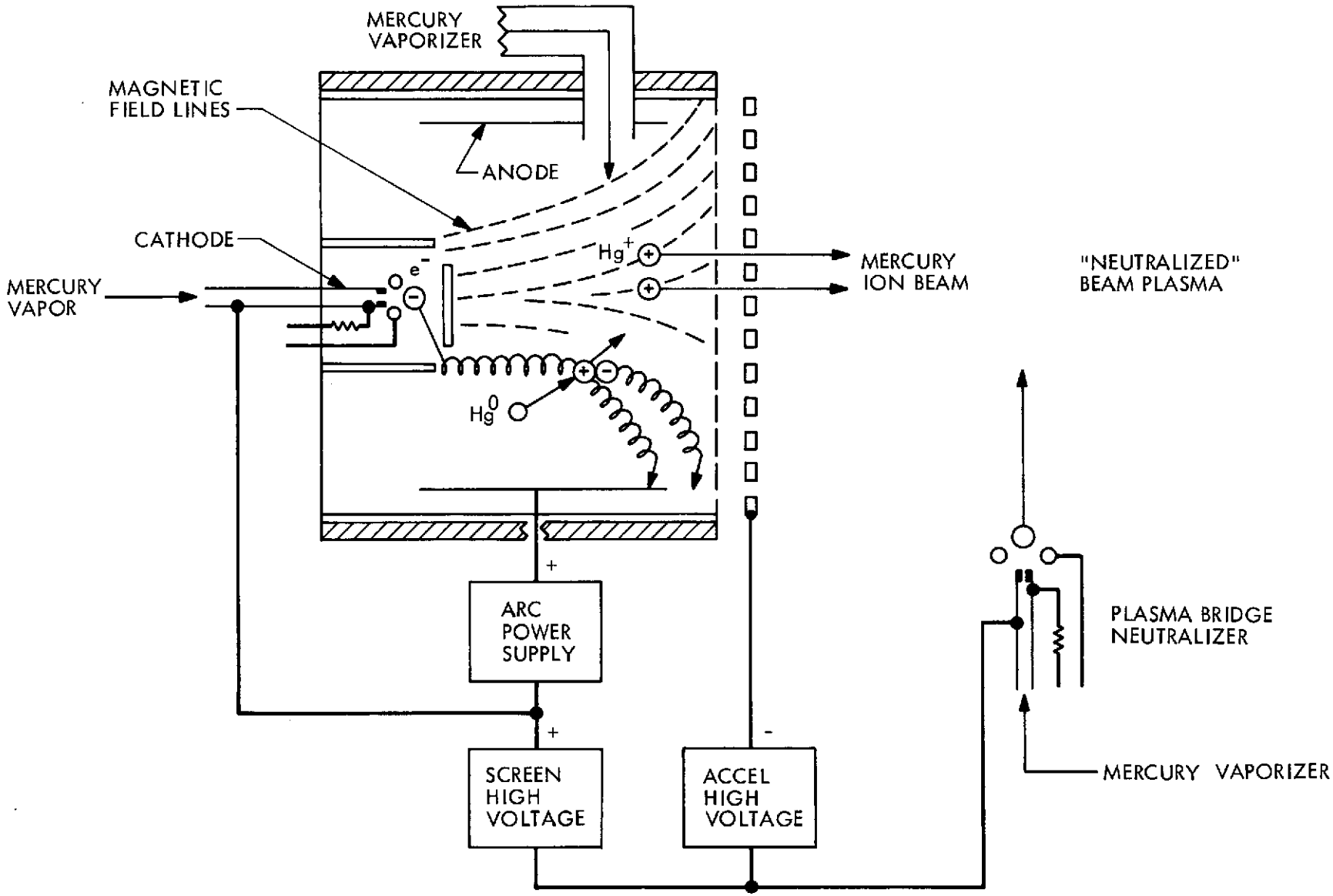

FIG. 2 SCHEMATIC OF THE THRUSTER SHOWING ION AND ELECTRON TRAJECTORIES

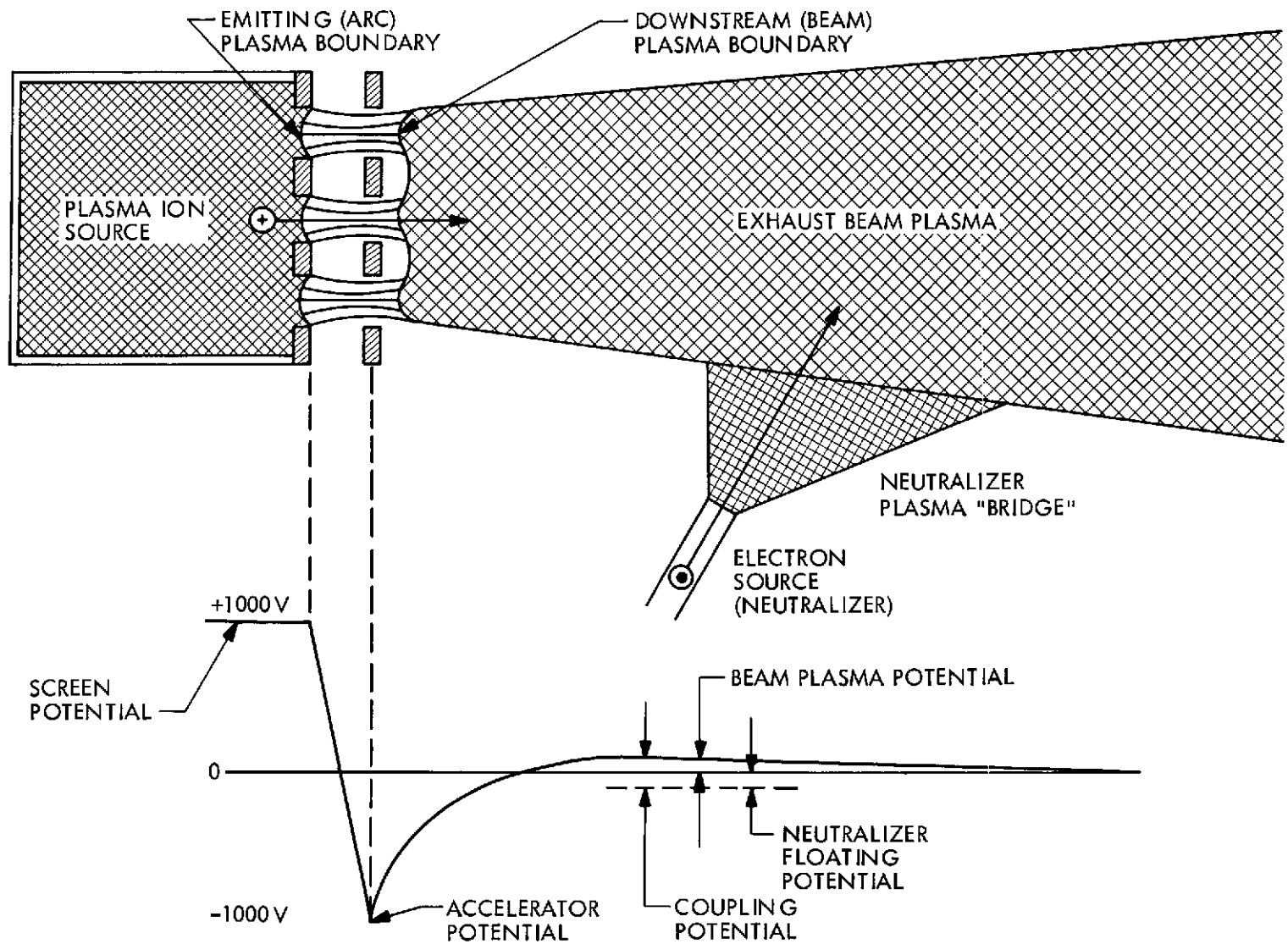

FIG. 3 SCHEMATIC OF ION ACCELERATION AND NEUTRALIZATION SHOWING DISTRIBUTION OF POTENTIALS

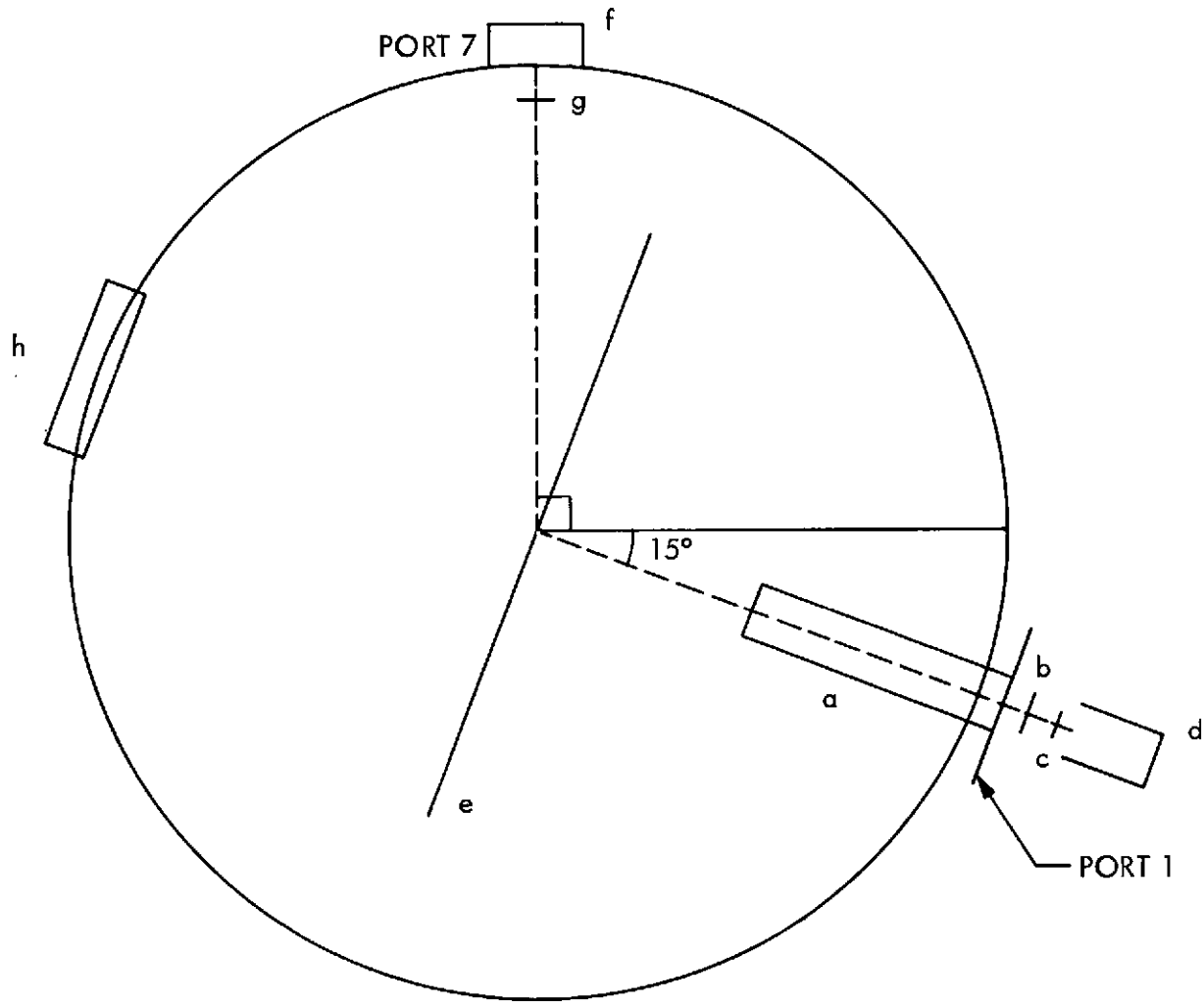

a. COLLIMATOR
b. FUSED QUARTZ VACUUM WINDOW
c. SALICYLATE COATED PYREX
d. PHOTOMULTIPLIER HOUSING
e. GIMBAL PLANE
f. XENON LAMP
g. FUSED QUARTZ VACUUM WINDOW
h. VACUUM PORT

FIG. 4 EXPERIMENTAL SETUP

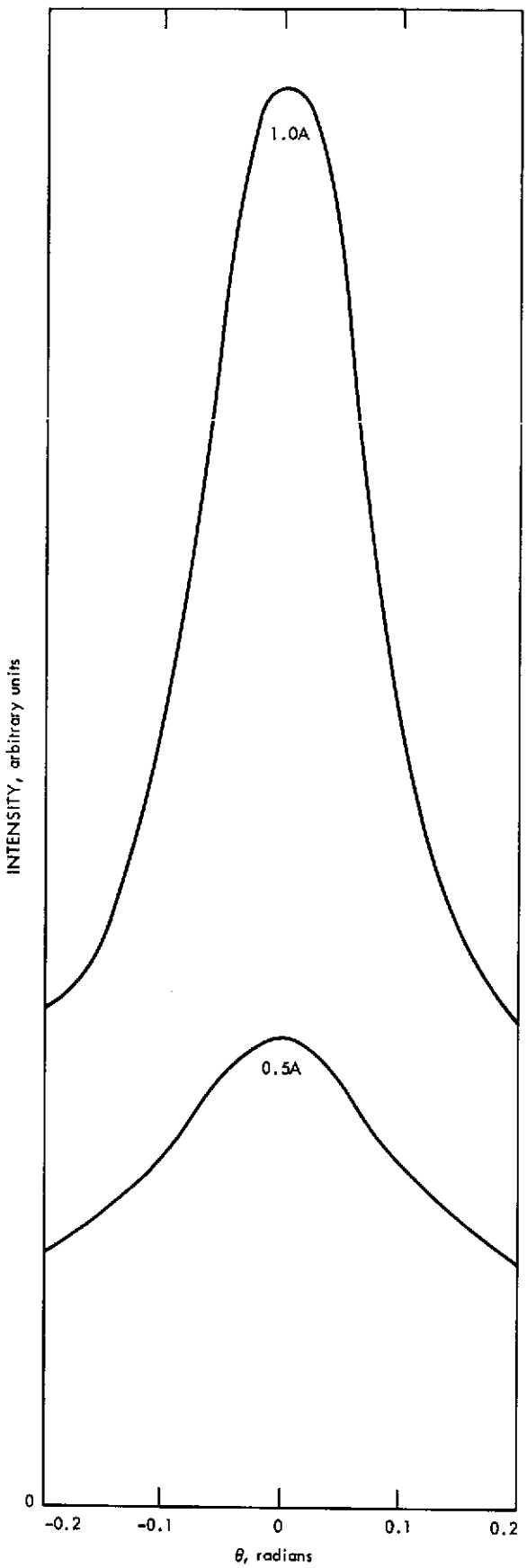

FIG. 5 INTENSITY PROFILES AT 1100 V SCREEN POTENTIAL AND 0.5 AND 1.0 A BEAM CURRENT

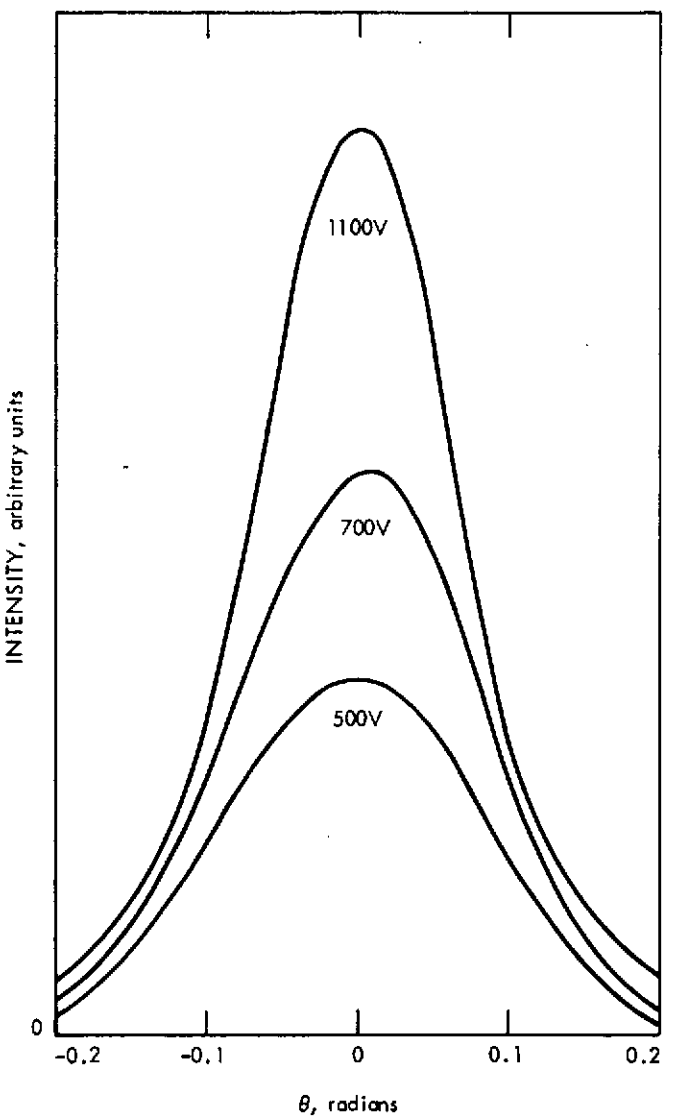

FIG. 6 INTENSITY PROFILES 1.0 A BEAM CURRENT AND 500, 700, and 1100 V SCREEN POTENTIAL; BACKGROUND HAS BEEN SUBTRACTED FROM THE SIGNAL

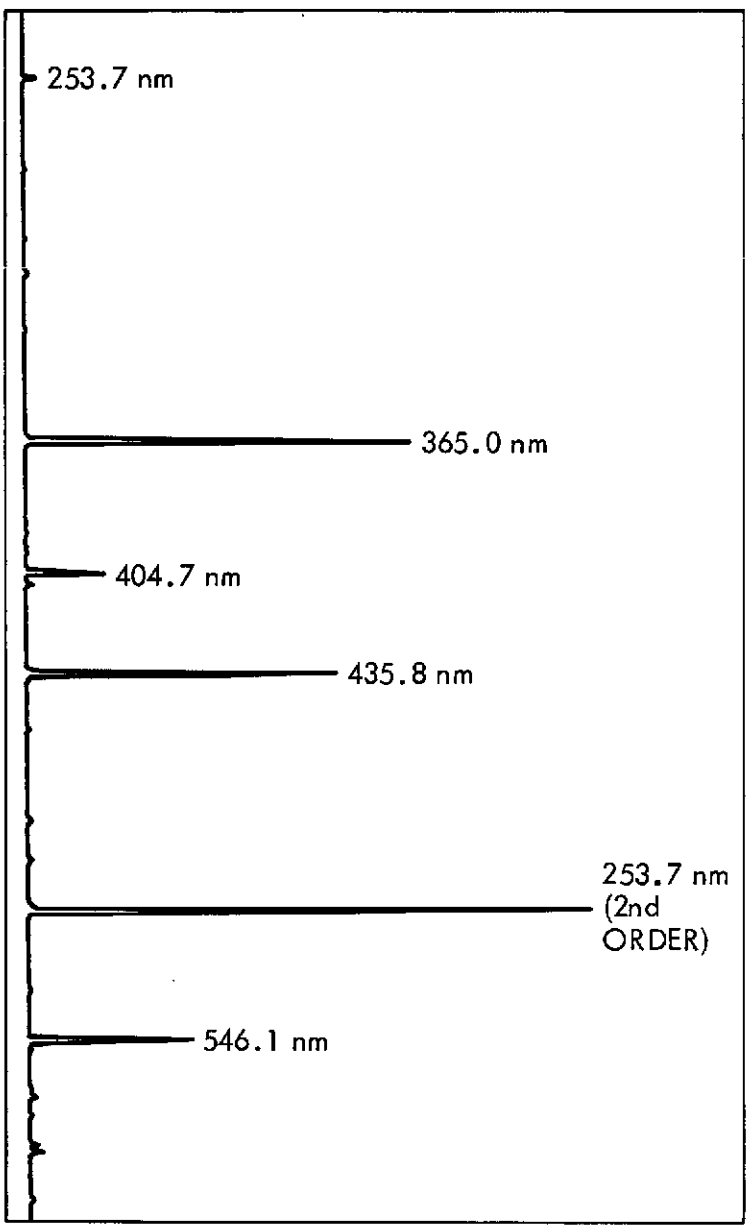

FIG. 7 SPECTRUM OF THRUSTER BEAM AT 0.5 m AXIAL DISTANCE AND 1.0 A BEAM CURRENT. THE HgI 253.7, 365.0, 404.7, 435.8, and 546.1 nm LINES ARE IDENTIFIED IN FIRST ORDER.

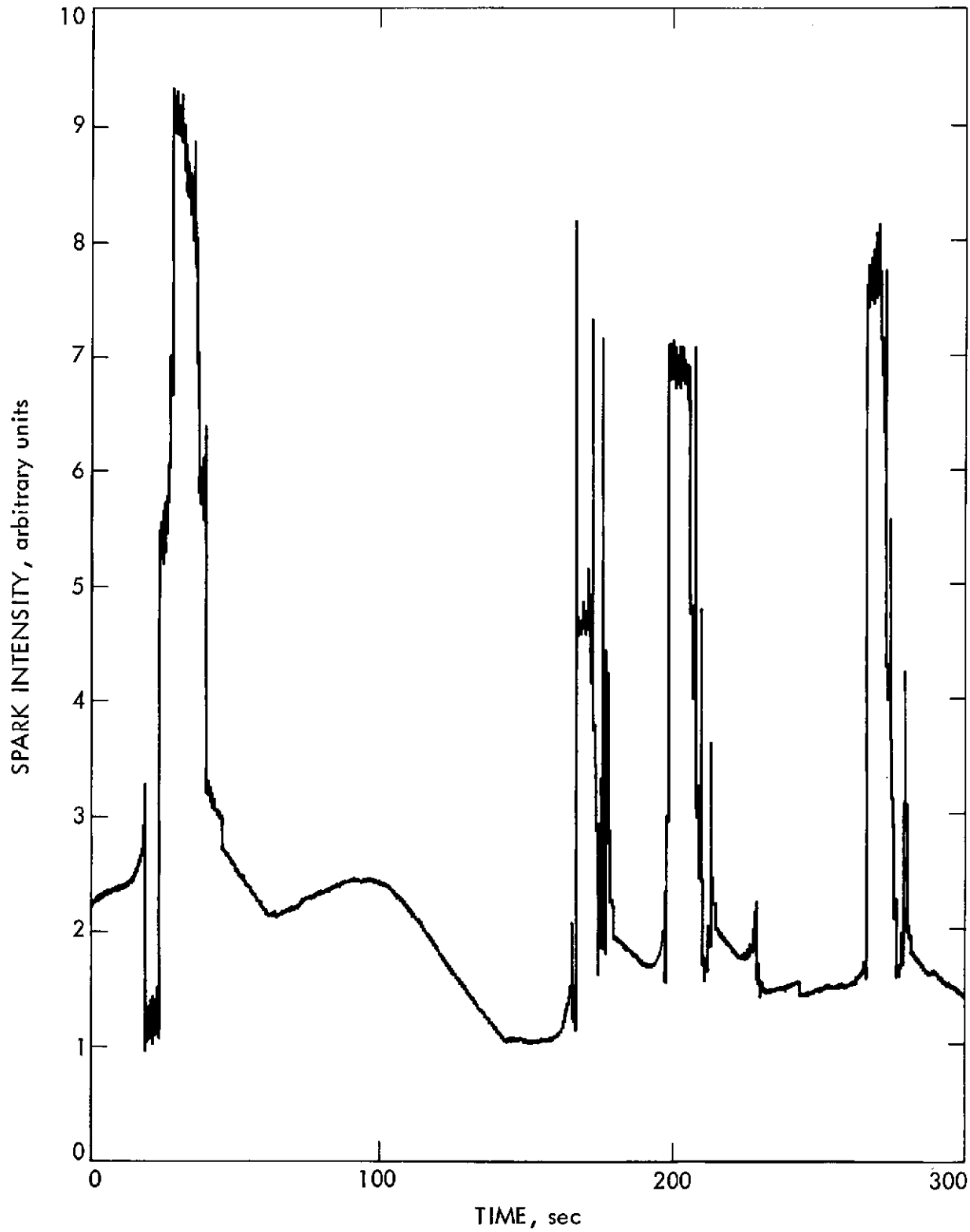

FIG. 8 ARCING WITH HIGH VOLTAGE ON

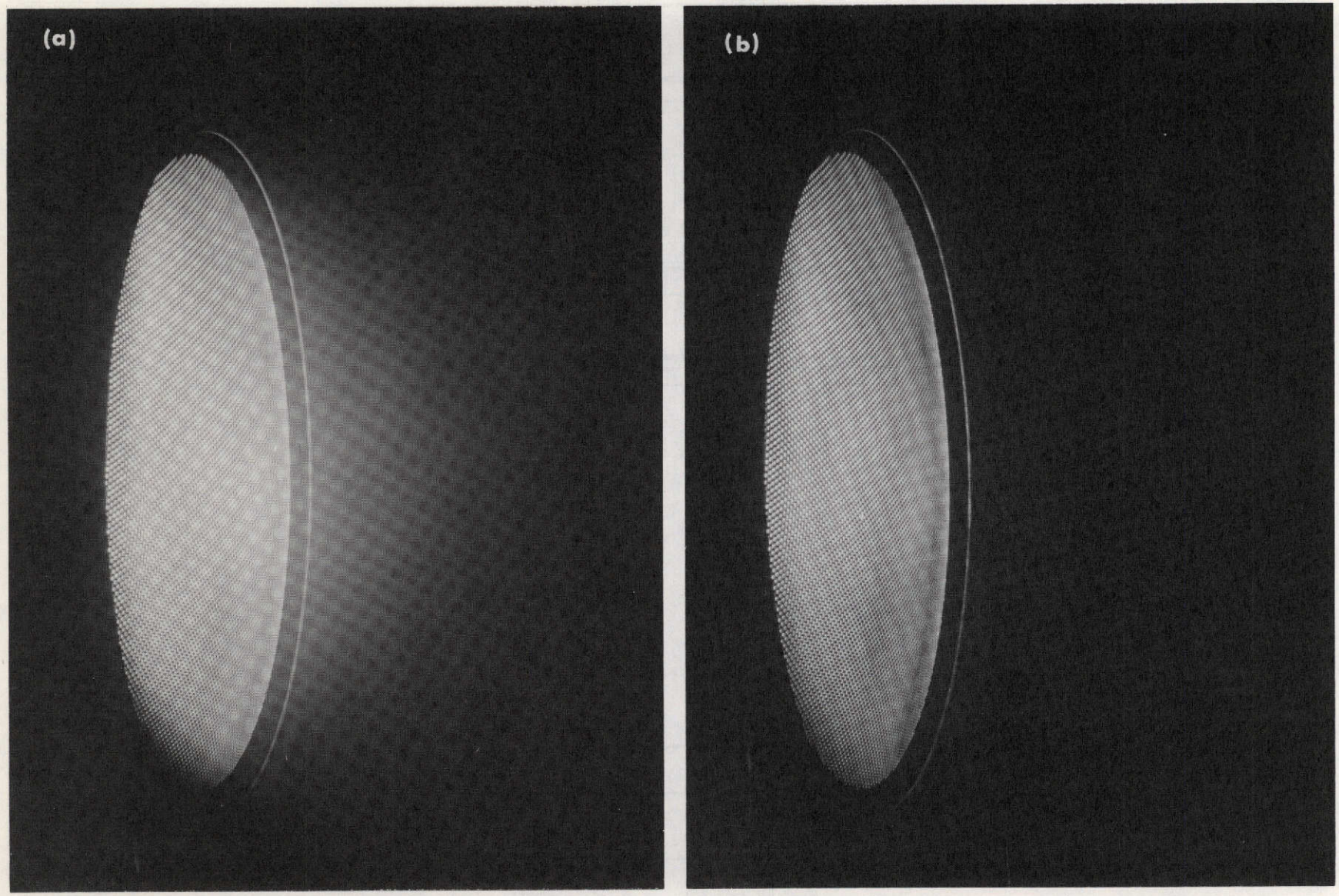

FIG. 9 OPERATING 30cm MERCURY ION THRUSTER: a) ARC ON WITH BEAM OFF, b) ARC AND BEAM ON

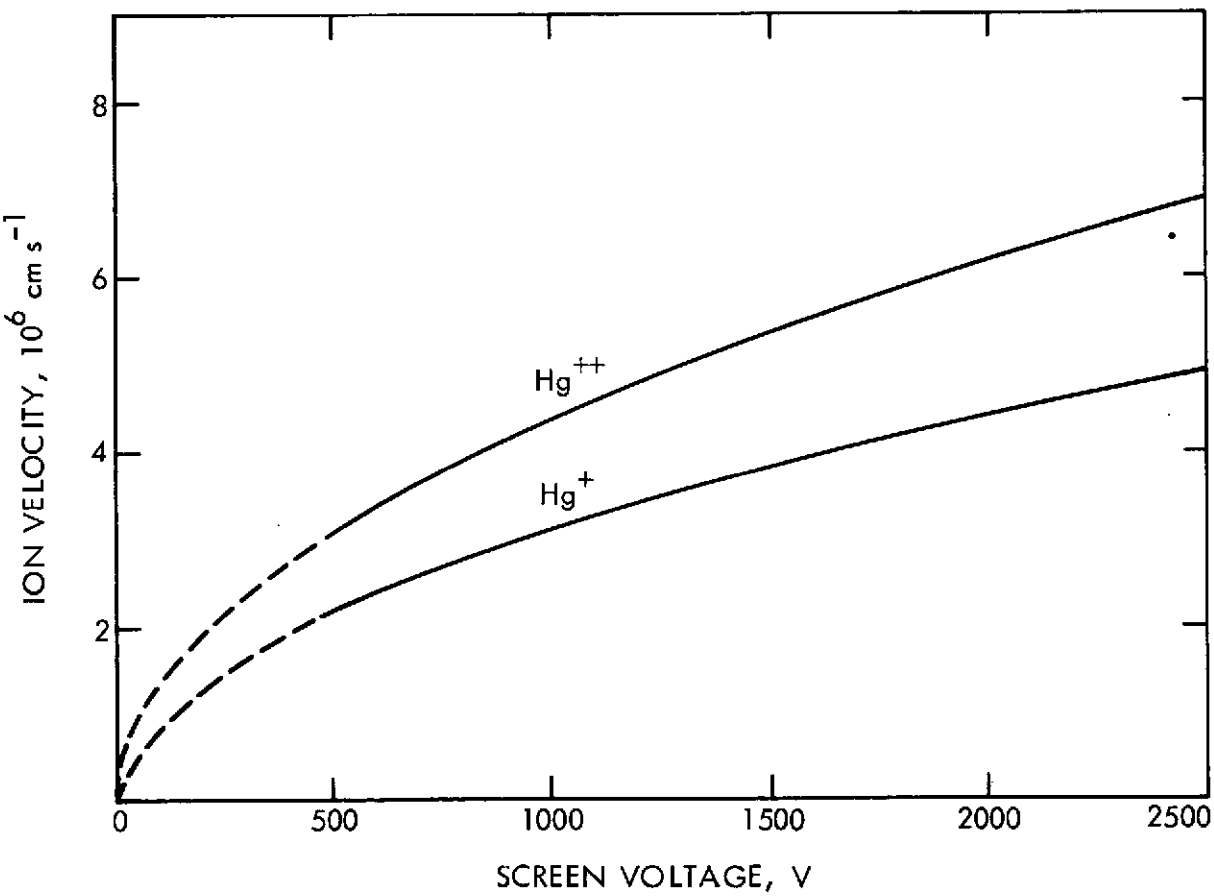

FIG. 10 ULTIMATE VELOCITIES OF SINGLY AND DOUBLY IONIZED MERCURY ATOMS

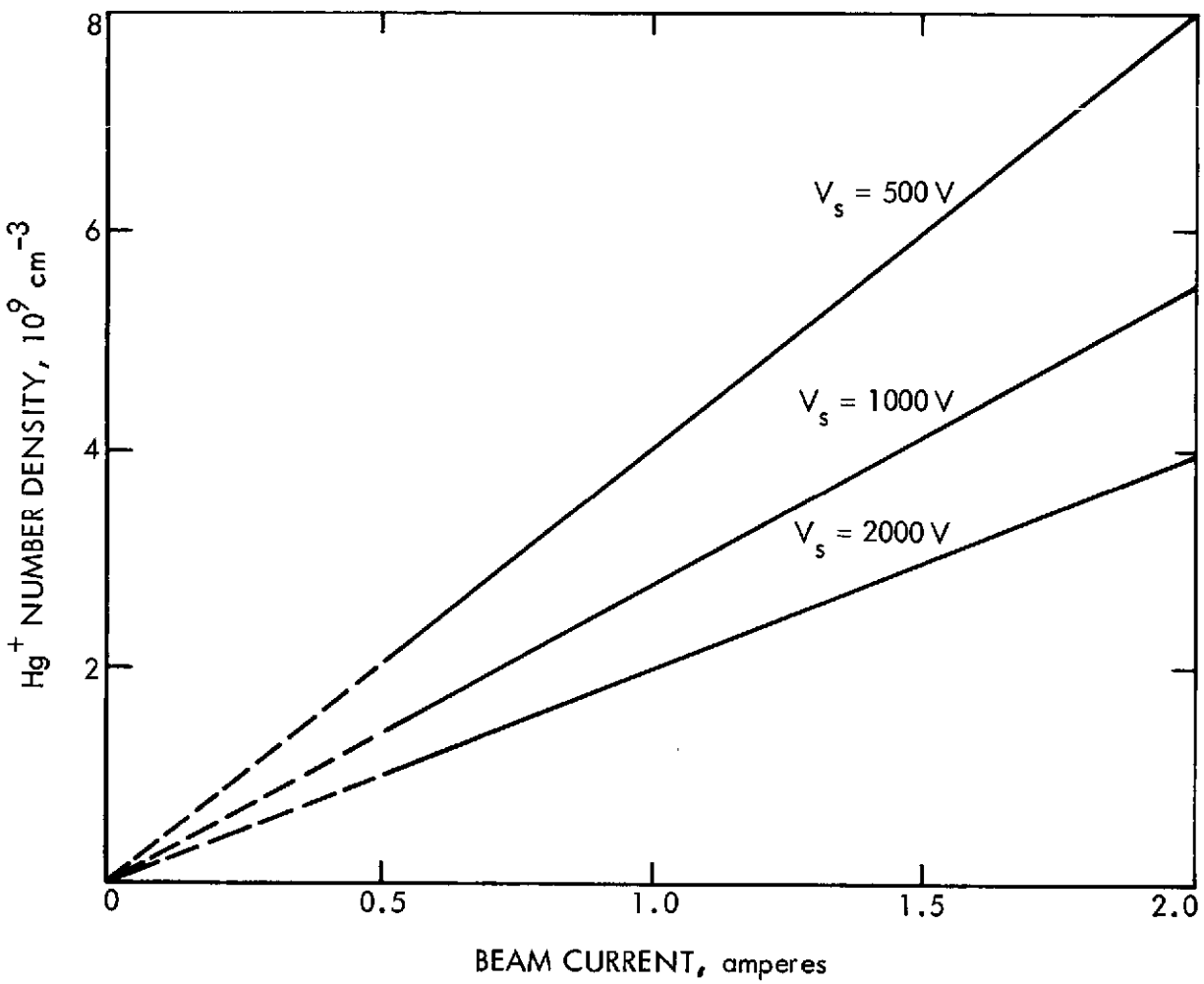

FIG. 11 NUMBER DENSITIES OF SINGLY IONIZED MERCURY ATOMS AT THE THRUSTER EXIT

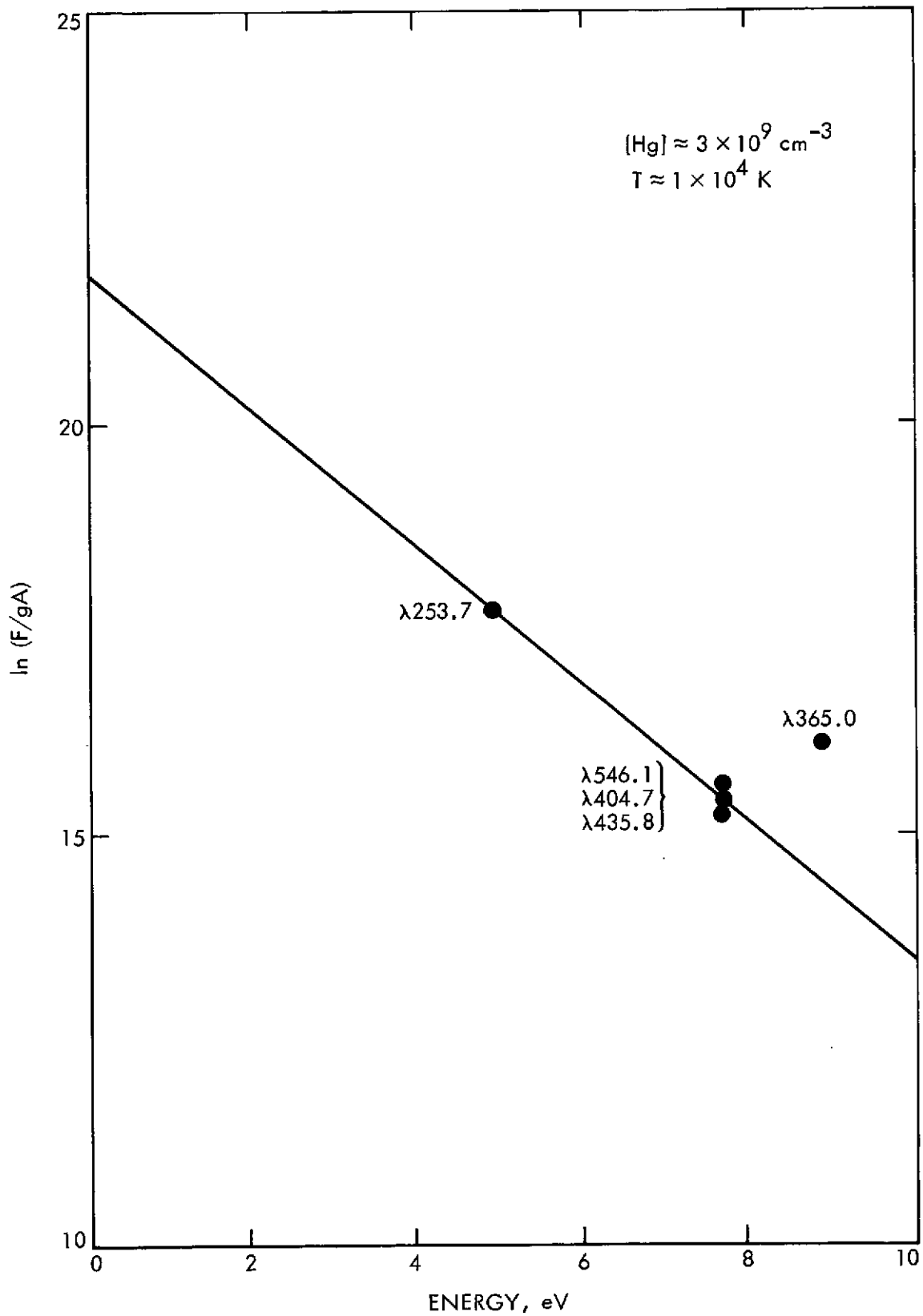

FIG. 12 EINSTEIN-BOLTZMAN PLOT OF THE NEUTRAL LINE INTENSITY DATA AT 2.0 m WITH THE PARTITION FUNCTION Z ≈ 1

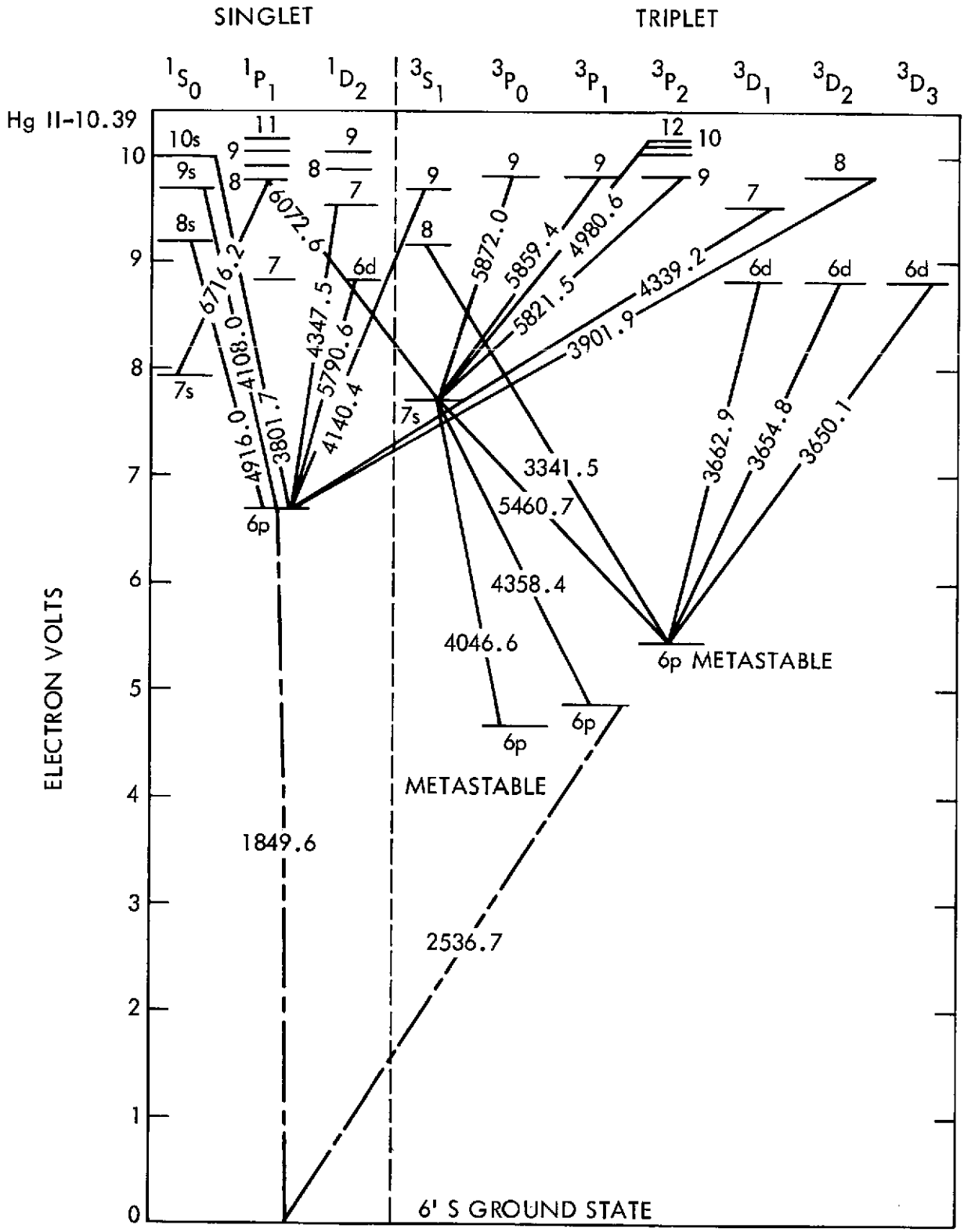

FIG. 13 ENERGY LEVEL DIAGRAM FOR HgI

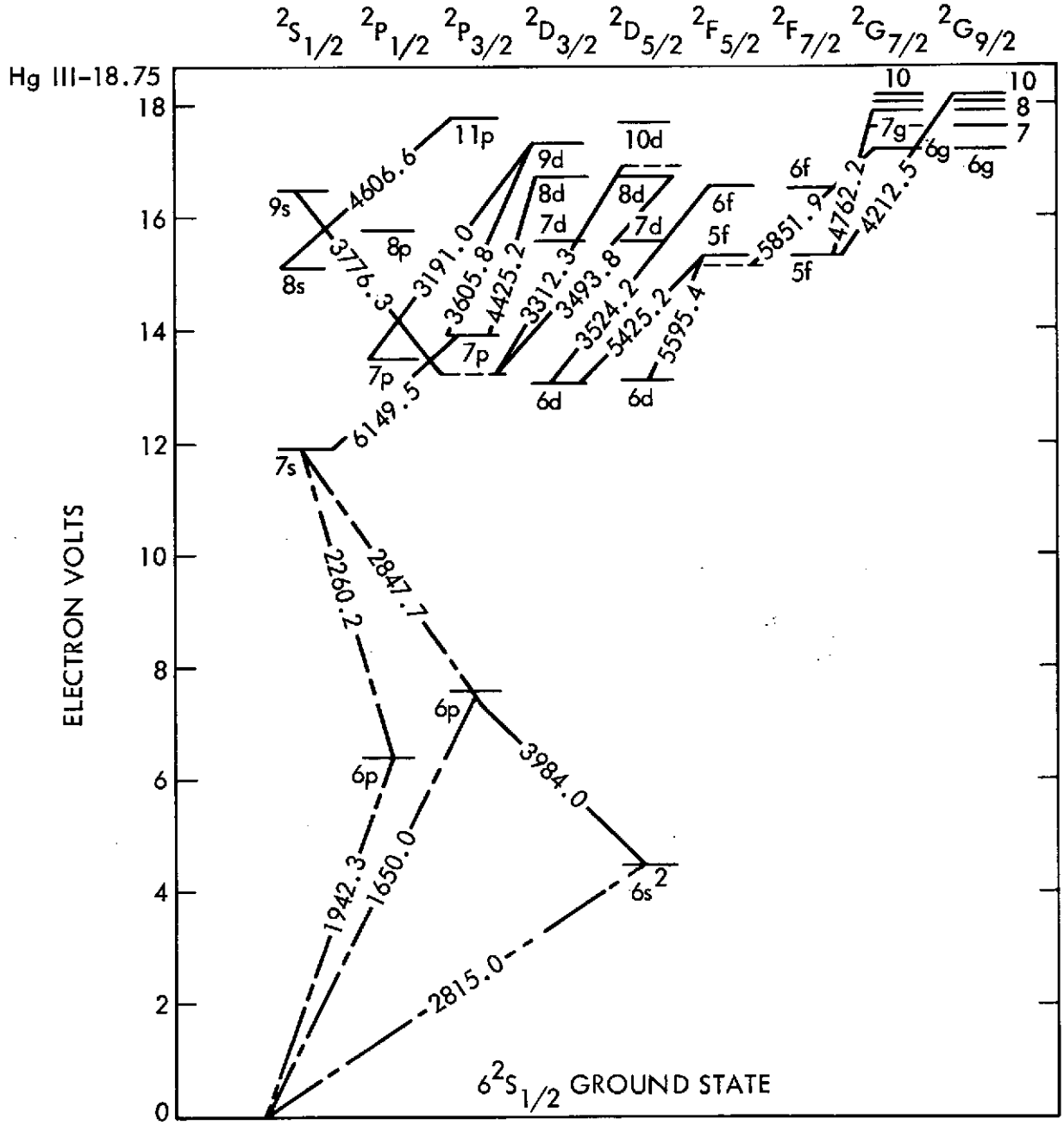

FIG. 14 ENERGY LEVEL DIAGRAM FOR HgII

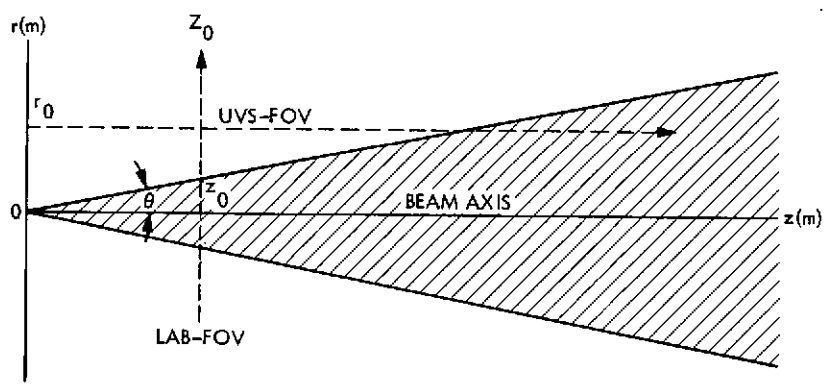

FIG. 15 COORDINATE SYSTEM USED TO CALCULATE APPARENT EMISSION RATES